

# MET: A Magneto-Inductive Sensing Based Electric Toothbrushing Monitoring System

Anonymous Author(s)

## ABSTRACT

Electric toothbrushes are widely used for home oral care, but many users do not achieve desired oral hygiene results due to incorrect brushing techniques or insufficient brushing coverage. Existing monitoring systems of electric toothbrush fail to detect these issues because they cannot achieve fine-grained position tracking. In this paper, we present a novel electric toothbrushing monitoring system called MET that tracks brushing coverage for all the 15 surfaces of teeth and detects different types of incorrect brushing techniques. This design is inspired by our observation that the motor inside an electric toothbrush generates a unique magnetic field, which can serve as a reliable signal for position and orientation tracking. MET is the first system that tracks the 6 degrees of freedom pose of an unmodified electric motor using magnetic inductive sensing. Experiments with fourteen users show that the average toothbrushing surface recognition accuracy of MET is 85.3%. Moreover, MET is robust to user location changes and posture variations and does not require any training from the users. Experimental results also demonstrate our significant advantages over existing commercial systems.

## 1 INTRODUCTION

As one of the most widely used home oral hygiene devices, a typical electric toothbrush (ET) uses a motor to generate rapid automatic bristle motions that can effectively remove plaque, reduce gingivitis, and prevent tooth decay and gum diseases [23, 41]. However, many users still develop dental problems even after using electric toothbrushes on a daily basis [75], and some users even experienced receding and bleeding gums, eroded enamel, and fillings falling out [16]. This is because they make some common mistakes, such as missing surfaces of some teeth, brushing with incorrect techniques, and brushing for insufficient or excessive time. The automatic detection of improper brushing habits can significantly improve the user’s oral hygiene results.

Existing ET monitoring systems have employed a variety of sensors, including camera [79], microphone [43], and inertial sensors [48]. The most advanced Oral-B GENIUS 7000 model uses a mounted smartphone camera to detect which one of the four quadrants that a user is brushing [9]. Nevertheless, it cannot tell which surfaces are being brushed within a tooth quadrant, not to mention the insufficient or over brushing, because the camera cannot see inside the user’s mouth. Moreover, the camera-based approach does not work in low light conditions and often raises privacy concerns. Some other systems like Philips and Kolibree rely

on inertial sensors to detect brushing areas [6, 11]. However, inertial sensor-based solutions usually suffer from low recognition accuracy due to drifting errors, and our experiments showed that the strong ET vibrations significantly aggravate the drifting errors of IMU-based positioning. Similarly, previous research on manual toothbrushing monitoring using motion features [39] does not work for ET due to its significant motion noise. As we can see, these sensing techniques have intrinsic limitations, and it is very challenging to build a monitoring system that monitors finer-grained surface coverage and incorrect brushing techniques reliably.

In this paper, we describe MET: a Magneto-Inductive Sensor based ET monitoring system, by exploiting a different sensing modality: magnetic field sensing. From extensive experiments, we observed that the motor of an ET generates a sub- $\mu T$  level quasi-static magnetic field around the brush. Although the strength of this magnetic field is weak, it has its unique frequencies and patterns that allow us to differentiate it from the ambient magnetic field. This offers a reliable and accurate indicator for toothbrush positioning as the field is robust to obstructions, e.g., human arms and non-line-of-sight conditions. Therefore, we build a magneto-inductive sensor using customized induction coils, which capture the time-varying magnetic flux density generated by the motor at specific frequencies. Previous research employs magnetic sensing for localization [24, 55, 57, 66, 68, 78], engine monitoring [61], and vehicle detection [34, 38]. Our work is different as we are the first to develop a position tracking system for an electric motor, which serves as a non-cooperative target in toothbrushing monitoring.

We develop a set of technologies to track the 6 Degrees of Freedoms (6 DoF) pose of electric toothbrush from scratch. Specifically, we construct an analytic magnetic model for the motor based on a point magnetic source that has a time varying magnetic moment. This model enables us to track the motor’s 5 DoF pose (3D position, yaw and pitch angles) based on magnetic sensor measurements. We note that this model is insensitive to the motor’s roll angle changes, so we also design a collaborative sensing algorithm that estimates the roll angle of the motor based on the unique signal waveform features. We design unsupervised learning algorithms to recognize brushing surfaces under user mobility. we develop an expectation-maximization based algorithm that iteratively estimates the toothbrushing surfaces. Although MET cannot sense the location and head pose of a user, it can infer these movements from toothbrush motion patterns and directions during brushing indirectly. Such techniques can be applied

in a broader setting to recognize activities and correlated context simultaneously.

Our design targets the rotation-oscillation based toothbrush, represented by Oral-B [9] that has the largest market share [17]. In a set of experiments with fourteen users, MET achieves a surface recognition accuracy of 85.3%, and detection accuracy of 92%, 87%, and 94% for aggressive, over, and insufficient brushing, respectively. Compared with commercial toothbrushing monitoring systems Oral-B and Phillips that use the camera and inertial sensors, MET also demonstrates significantly higher detection accuracy.

The contribution of this work is summarized as follows.

- We build MET - an electric toothbrush monitoring system that can reliably track brushing coverage for 15 surfaces of teeth and detect incorrect brushing.
- To the best of our knowledge, this is the first work to perform 6 DoF pose tracking based on the sensing and modeling of the magnetic field of an unmodified electric motor. Previous studies on motor magnetic field primarily focus on motor status monitoring, and magnetic signature and noise modeling [33, 76], but these works do not provide solutions to achieve 6 DoF pose tracking.
- We create a set of technologies to track fine-grained toothbrushing activity, including 1) an analytic magnetic model to approximately characterize the complex magnetic field generated by the toothbrush motor; 2) a collaborative sensing scheme to detect motor roll angle based on a signal waveform model; 3) a training-free surface recognition algorithm that infers brushing surfaces under user movements, e.g., location changes and head posture variations, based on correlated toothbrush motion direction and orientation changes.
- Experimental results with fourteen users show that MET achieves average toothbrushing surface recognition accuracy of 85.3%, outperforming other state-of-the-art systems significantly.

## 2 OVERVIEW

### 2.1 ET Monitoring Systems

The electric toothbrush manufacturer recommends holding the brush head against each tooth for a few seconds, then slowly moving on to the next one. Repeat the process for the outer, chewing, and inner surfaces [3, 4]. The entire toothbrushing session should last for two minutes, and every surface of the teeth should be covered evenly. Although the procedure is straightforward, users still make many mistakes: 1) insufficient brushing. Clinical studies show that insufficient brushing for tooth surfaces, especially the inner surfaces of the back teeth, is among the most common improper brushing habits. If not cleaned regularly, these back molars are prone to develop dental decay quickly and may require extraction [1, 52, 54, 69]. 2) Over-brushing. Due to the high-frequency motions of bristles, brushing a surface for too long can cause tooth sensitivity and receding gums [25].

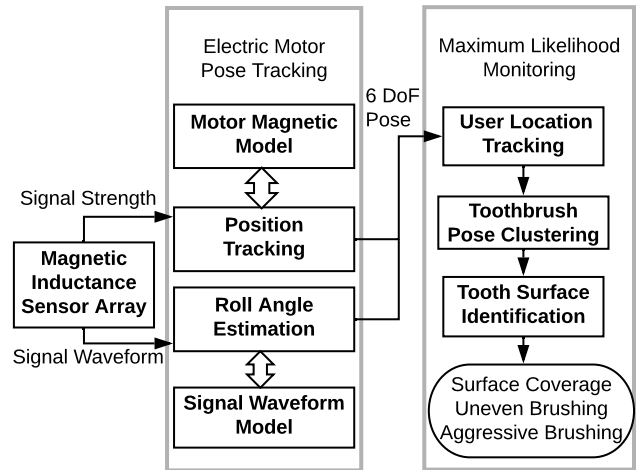


**Figure 1: System Overview**

3) Incorrect brushing motions. Aggressive brushing, such as the vigorous back and forth brushing motions in long strokes, is not effective in removing plaques and can injure the gum [5, 37].

To monitor the toothbrushing process, it requires high precision to differentiate the subtle direction and orientation changes. Existing ET monitoring systems rely on multiple types of sensors, including a camera, microphone, and inertial sensor. However, all these sensors have major limitations, such as visibility blockage or motion noises. For example, the state-of-the-art Oral-B toothbrushing monitoring system that is based on camera can only achieve a rough-grained monitoring, i.e., quadrant level, which is still insufficient for detecting blind spots and missing surfaces.

In this paper, we identify that the magnetic field generated by the electric motor serves as a reliable pose tracking signal. While such a magnetic field generated by electric appliances is usually treated as noise in previous research [33, 76], we initiate the study to understand the spatial distribution of the motor magnetic fields and use them to achieve position and orientation tracking. Our electric motor tracking technique enables a more fine-grained toothbrushing monitoring than existing technologies.

### 2.2 System Design and Challenges

Figure 1 shows an overview of our monitoring system design. Our design has three major components: the sensor hardware, the motor pose tracking models and algorithms, and the algorithms to monitor toothbrushing surfaces and techniques. These three components and their associated challenges are discussed as follows.

**Hardware for Motor Magnetic Field Sensing.** Our initial experiments showed that the magnetic field from the Oral-B genius 7000 has a strength that ranges from approximately  $5nT(10^{-9})$  to  $1\mu T(10^{-6})$ , and the primary harmonic of the time-varying magnetic field is about 1000 Hz. A typical home environment typically causes a constant background magnetic field that ranges from about  $50\mu T$  to hundreds of

$\mu T$ . It is challenging to sense the electric toothbrush motor magnetic fields in a high-fidelity, reliable, and low-cost way. We have considered alternative sensor design options, as detailed in Section 6. We eventually custom-built magnetic inductance sensors to meet the specific sensing resolution and bandwidth requirements for the motor magnetic fields. **Motor Pose Tracking.** The magnetic field generated by the DC motor provides rich information on the position and orientation of the toothbrush. However, it is a complex field generated by the multiple poles of the rotor, and each pole functions as a electric magnet with time-varying position, orientation, and magnetic strengths. It is very challenging to model this field to support motor position tracking.

*Modeling the Motor Magnetic Field Strength.* Magnetic field strength modeling of DC motor is not new. Many previous works employ the Finite Element Method (FEM) to analyze the magnetic field [21, 26, 30, 80]. However, these works only focus on analyzing the magnetic fields inside of the motor, not the magnetic field outside the motor. Furthermore, the FEM technique requires detailed parameters of the motor, such as the strength of the internal magnets and the permeability of the electromagnet cores. Such proprietary information is not available for the DC motor in an electric toothbrush due to the private implementation. The FEM also has a large computation complexity, which makes it difficult to achieve real-time monitoring in our application. In this paper, through extensive experiments, we construct an approximate motor magnetic model with sufficient accuracy but with significantly lower computation complexity than the FEM model. In particular, we model the motor as a point magnetic source with a time-varying magnetic moment, and validate it with empirical data. Based on this model, we developed a tracking algorithm for the 5 DoF pose of the motor, i.e., 3D position, and pitch and yaw angles.

*Modeling the Motor Magnetic Field Waveform.* The toothbrush roll angle is crucial information to enable brushing surface recognition [39, 47], yet we shall see in Section 3.2, the change of roll angle has little impact on the magnetic field strength. To track an object’s orientation using magnetic sensing, previous approaches typically rely on specialized magnetic field sources, such as a regular-shaped magnetic tag or magnetic coils with sinusoidal currents [19, 28, 60]. In our system, we avoid modifying the electric toothbrush for the sake of user convenience. We bring the unique perspective that the magnetic field signal waveforms have subtle changes according to the roll angle. We developed a new technique that measures the similarities between the sensor measurements and template waveforms, and combine the data from multiple sensors to achieve a coarse-grained the toothbrush roll angle estimation.

**Toothbrushing Monitoring.** Even with the 6 DoF pose tracking, it is not enough to recognize each brushing surface and detect various brushing mistakes. The primary challenge is that each user is not standing still during brushing.

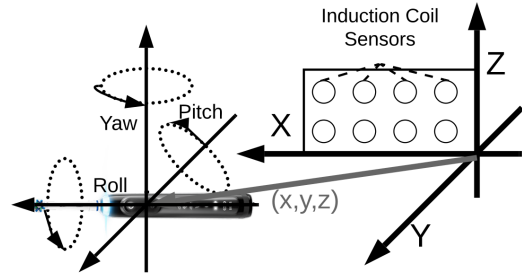


Figure 2: The Coordinate System

A user can stand at different locations near a sink for different brushing sessions. During each brushing session, a user may naturally change brushing gestures, turning head, and even change locations around the sink. The key insight that enables toothbrushing surface recognition is that the tooth surfaces still maintain their relative positions regardless of the user movements, so we describe such relative positions using a tooth map. Based on the tooth map, we design a novel Expectation-Maximization based algorithm that iteratively estimates the most likely brushing surface, and a Hidden Markov Model (HMM) based algorithm to estimate the user’s most-likely movements.

### 2.3 System Deployment

As shown in Figure 2, the sensor is mounted near the sink on one side of a user with at the appropriate height, this is similar to the Oral-B monitoring system that requires mounting a smart phone (camera) in front of the user. We assume a user conducts a toothbrushing session over a sink for rinsing and cleaning to prevent drooling everywhere, which is recommended for electric toothbrushing in general [18, 22, 35]. MET does not require any training from its users, because all the tracking and recognition algorithms can be calibrated and trained by the developer before deployment.

MET alerts its user in real-time when it detects over brushing and back-and-forth incorrect brushing techniques. By the end of each brushing session, it reminds the user if he or she forgets to (or insufficiently) brush any of the 15 surfaces of teeth. It also generates a post-brush report with detailed information on the brushing surface sequence and duration. Such monitoring functions are useful for general users. Moreover, dentists can provide personalized brushing recommendations to the patients, and the patients want to know if their toothbrushing is adequate and correct while they are at home. Children and teens who need training and real-time assistant to develop good toothbrushing habits can also benefit from it.

To monitor toothbrushing, it is essential to track the 6 Degrees of Freedom pose of the toothbrush, which includes 3 DoF of position and 3 DoF of orientation. To describe the 6 DoF pose, we introduce the coordinate system as shown in Figure 2. The Z axis is pointing vertically up, the X axis points to the user, and Y axis points to the right of the user. The 3 DoF orientation of the toothbrush is described using the Tait-Bryan convention. Specifically, the initial orientation of

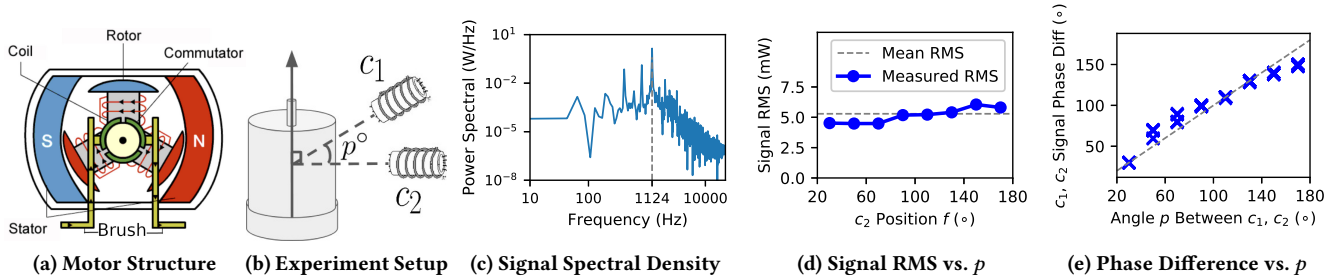


Figure 3: Electric Motor Magnetic Field Characteristics

the toothbrush is parallel to the X axis. Any orientation can be obtained by consecutively rotating the toothbrush around X axis (roll), around Y axis (pitch), and around Z axis (yaw).

### 3 MOTOR MAGNETIC MODEL AND 5 DOF POSE TRACKING

In this section we firstly construct a model that can estimate the magnetic field distribution around the motor. Using this model, we develop a positioning algorithm to track the 5 DoF pose based on magnetic sensor measurements.

#### 3.1 Electric Toothbrush Motor

An Oral-B 7000 ET relies on a brushed direct current (DC) motor to generate high-speed rotary motions. The DC motors usually have private implementation, but the general structure is the same. As shown in Figure 3a, a DC motor contains two sectors of permanent magnets. The rotor contains three poles, which generate magnetic field using the magnetic coils. Part of the rotor is a commutator that connects the coils to the electric brush. As the commutator rotates with the rotor, its connection with the electric brush changes, causing the reverse of the currents, which generates a torque with a constant direction. The periodic motions of the rotors and the switching of the electric brush generate a complex and discontinuous magnetic signal [29, 71, 72], whose main harmonic is correlated with the motor rotation rate [46].

#### 3.2 Empirical Study

We conduct experiments to understand the magnetic field generated by a motor, and the experimental setup is illustrated in Figure 3b. We place two magnetic sensors around an electric motor. The two sensors are in a plane perpendicular to the motor axis. They have the same distance to the motor center, and they are apart by an angle  $p$ . We record magnetic signals when the angle  $p$  changes. From this experiment, we make the following observations.

**Signal Periodicity.** When we analyze the magnetic signals collected at different locations, we find that the signals are highly periodic, with a constant signal frequency. When we plot the signal power spectral density, we can see a large peak around the frequency of 1124 Hz. An example is shown in Figure 3c.

**Signal Strength Isotropy.** Next, we record the signal strength of the coil  $c_2$ , measured by root mean square (RMS) when the coil  $c_2$  is placed at different angles  $p$ . We plot the

recorded RMS when the angle  $p$  changes in Figure 3d. We can see that the RMS remains stable, with only small fluctuations.

**Signal Phase Difference.** We compute the signal phase difference by finding the peak value of the cross-correlation between the signals from  $c_1$  and  $c_2$ . The results are shown in Figure 3e. We can see that when the two coils are at an angle  $p$  apart, the signal phase difference is also approximately  $p$ .

#### 3.3 Motor Magnetic Model

We use  $s(p, t)$  to denote the sensor measurement collected at angle  $p$  at time  $t$ . To summarize the above three observations, we can approximate the signal  $s(p, t)$  using  $|M| \cos(\omega t - p)$ . In particular,  $s(p, t)$  can be approximated by a sinusoidal function because of the first observation: the signal is highly periodic. The signal has a constant amplitude of  $|M|$  because of the second observation: the signal has approximately the same magnitude regardless of the angle  $p$ . And the signal has a phase of  $p$  because of the third observation. One feasible model of the magnetic field source that satisfies all the three observations is shown as follows. (We assume the motor axis is in parallel to the x-axis as described in Figure 2):

$$M_0(t) = |M|[0, \cos \omega t, \sin \omega t]^T. \quad (1)$$

The model described by Equation 1 suggests that we can replace the electric motor with a point magnet with a magnetic moment of  $M_0(t)$ , and the magnetic sensors will still have similar measurements.

#### 3.4 Sensor Measurement Model

Based on the motor magnetic model described in Equation 1, we can deduct a sensor measurement model based on the magnetic field distribution equations. The problem is illustrated in Figure 2. A induction coil sensor is installed at a known position  $[a, b, c]$ . The model predicts the sensor measurements when a motor that generates a magnetic moment  $\vec{m}(t)$  changes its position  $[x, y, z]$ , pitch  $\beta$  (rotation along the y-axis) and yaw  $\theta$  (rotation along the z-axis).

**The Influence of Orientation Changes.** As shown in Figure 2, we consider the toothbrush's initial orientation as being parallel to the positive direction of the x-axis. The influence of these rotations can be regarded as rotations on the initial magnetic moment  $M_0(t)$ . We use rotation matrices  $R_z(\theta)$  and  $R_y(\beta)$  to represent the yaw and pitch rotation operations. Then we can obtain the magnetic moment  $M(t)$  after rotation in the following equation:

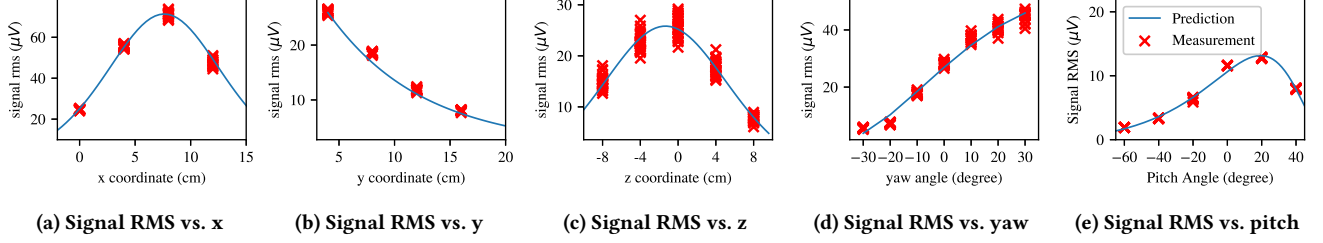


Figure 4: Magnetic Sensing Model Validation

$$M(t) = R_z(\theta)R_y(\beta)M_0(t),$$

$$R_z(\theta) = \begin{bmatrix} \cos \theta & -\sin \theta & 0 \\ \sin \theta & \cos \theta & 0 \\ 0 & 0 & 1 \end{bmatrix}, R_y(\beta) = \begin{bmatrix} \cos \beta & 0 & \sin \beta \\ 0 & 1 & 0 \\ -\sin \beta & 0 & \cos \beta \end{bmatrix} \quad (2)$$

**The Influence of Motor Position.** For an induction coil sensor installed at position  $[a, b, c]^T$ , its relative position from the motor to the induction coil is  $\mathbf{r} = [r_x, r_y, r_z]^T = [a-x, b-y, c-z]^T$ . The magnetic field  $B$  at the coil's position generated by a dipole  $M(t)$  can be calculated using following equation [19]:

$$B(\mathbf{r}, M(t)) = \frac{\mu}{4\pi|\mathbf{r}|^3} \left[ \frac{3\mathbf{r}\mathbf{r}^T}{|\mathbf{r}|^2} - \mathbf{I}_3 \right] M(t) \quad (3)$$

**The Induced Voltage in a Magnetic Coil.** According to Faraday's law of induction, the induced voltage  $v(t)$  at the induction coils sensor is linear to the derivative of the magnetic field. In our setting, all the induction coils are parallel to the Y axis, i.e.,  $\mathbf{s} = [0, 1, 0]^T$ . Substitute Equations 1, and 2 into 3, we can obtain the analytical expression of the received signal in an induction coil, as shown in Equation 4.

$$\begin{aligned} v(t) &= \omega N_{RX} A_{RX} \mu_{RX} B(\mathbf{r}, M(t)) \cdot \mathbf{s} \\ &= K[a_c(\mathbf{r}) \cos(\omega t) + a_s(\mathbf{r}) \sin(\omega t)] \\ a_c(\mathbf{r}) &= [\cos(\theta)(2r_y^2 - r_x^2 - r_z^2) \\ &\quad - 3r_y r_z \sin(\theta)] / (r_x^2 + r_y^2 + r_z^2)^{2.5} \\ a_s(\mathbf{r}) &= [\sin(\beta) \sin(\theta)(2r_y^2 - r_x^2 - r_z^2) + 3r_x r_y \cos(\beta) \\ &\quad + 3r_y r_z \sin(\beta) \cos(\theta)] / (r_x^2 + r_y^2 + r_z^2)^{2.5} \end{aligned} \quad (4)$$

In this equation,  $\omega$  is the magnetic signal angular velocity.  $K$  is a constant determined by  $N_{RX}$ ,  $A_{RX}$  and  $\mu_{RX}$ , which represent the number of rounds, area, and the magnetic permeability of the induction coil, respectively. The expressions for  $a_c(\mathbf{r})$  and  $a_s(\mathbf{r})$  are also provided.

**Model Validation.** According to equation 4, the RMS of the signal  $v(t)$  is linearly correlated with  $\sqrt{a_c^2 + a_s^2}$ . We conduct experiments to validate this relation. We place the electric motor at the locations with x coordinate ranges from  $[0, 12]$  cm, y ranges from  $[0, 8]$  cm, z ranges from  $[0, 8]$  cm, yaw angle from  $[-30^\circ, 30^\circ]$  and pitch angle ranges from  $[-60^\circ, 40^\circ]$ . Sample measurement results are shown in Figure 4. We can see that the prediction of the model closely matches the actual sensor measurements. The  $R^2$  value between the sensor measurements and the theoretical predictions of our model is 0.988, indicating the high accuracy of our model predictions.

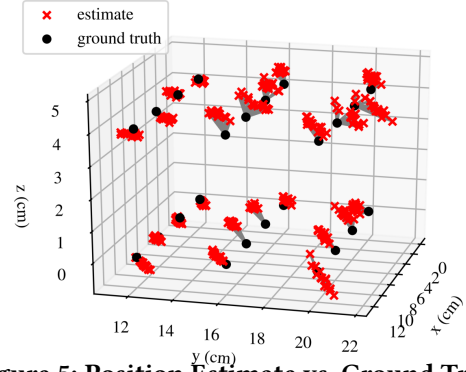


Figure 5: Position Estimate vs. Ground Truth

### 3.5 5D Pose Tracking

The algorithm to track the motor's 5D pose  $X = \{x, y, z, \beta, \theta\}$  works as follows. In our setting we have eight magnetic induction coil sensors, with each coil  $i$  installed at a known position  $[a_i, b_i, c_i]^T$ , at the same direction of  $[0, 1, 0]^T$ . At each time moment, the sensor array records the signal RMS  $\mathbf{v} = [v_1, v_2, \dots, v_8]$ . Then we can compute the motor's 5 DoF pose by solving the following optimization problem:

$$\begin{aligned} \min_X \quad & J = \sqrt{\sum_{i=1}^8 |v'_i - v_i|^2} \\ \text{s.t.}, \quad & v'_i = K \sqrt{a_c(\mathbf{r}_i)^2 + a_s(\mathbf{r}_i)^2} \\ & X_{min} \leq X \leq X_{max} \end{aligned} \quad (5)$$

In this equation,  $a_c(\mathbf{r}_i)$  and  $a_s(\mathbf{r}_i)$  are defined in Equation 4. We use a standard optimizer to solve this optimization problem. We plot a sample 3D position tracking results in Figure 5. In this figure, the black dots represent the ground truth coordinates, while the red crosses represent the estimated positions by our tracking algorithm. We can see that the tracking algorithm can distinguish different positions. The average tracking error is 2.9 cm, and the 90% percentile tracking error is 4.1 cm.

To calibrate the positioning algorithm, it is necessary to obtain parameters used in Equation 4, which include the position,  $[a, b, c]$ , and the magnetic parameters,  $N_{RX}$ ,  $A_{RX}$ ,  $\mu_{RX}$ , for each coil. While it is possible to measure these quantities directly, we found it easier to estimate them indirectly. In particular, we need to place the toothbrush at different known poses and obtain the sensor measurements. Then we use the maximum likelihood estimation technique, which estimates the parameters such that the difference between the magnetic field prediction of our model and the actual measurement is minimized.

## 4 ROLL ANGLE ESTIMATION

As illustrated in Figure 2, the roll angle represents how the toothbrush rotates around the axis of its handle. The accurate monitoring of the toothbrush’s roll angle is essential to reliable toothbrushing monitoring [39, 40, 49].

We conduct experiments to investigate how the roll angle influences the signal waveforms. We define the roll angle to be  $0^\circ$  when the toothbrush faces the coil with the brush head. We rotate the toothbrush and take measurements at different roll angles. Figure 6 shows the different magnetic signal waveforms captured by a single induction coil. We can see that when roll angles are  $90^\circ$  and  $270^\circ$ , the waveform contains small jitters (at 1 and 6 millisecond); this is caused by the large current changes during the electric brush switching. Whereas, the waveforms when roll angles are  $0^\circ$  and  $180^\circ$  are inverse to each other: when the upper signal has small peaks at 1 and 6 milliseconds, the lower signal has small valleys at the same moments.

Based on these unique signal characteristics and patterns generated by the motor, we design a collaborative sensing algorithm to recognize the toothbrush roll angle. Note that different sensor coils can collect different waveforms of the magnetic signal because they have different roll angles relative to the toothbrush, this algorithm needs to fuse sensing data from multiple coils to obtain the final roll angle recognition result. The basic ideas for recognizing the electric motor roll angle are as follows. At each moment, the sensor array collects eight signal waveforms. Then a customized signal similarity measurement function is used to calculate the similarities between the collected signal waveforms and the template signal waveforms. These signal similarities measurements serve as inputs to a deep fully connected neural network to recognize the toothbrush roll angle.

We firstly collect a list of template signals  $\{t_1, t_2, \dots, t_M\}$ , where  $t_m$  represents the magnetic field signal collected by the sensor when the toothbrush has a roll angle of  $r_m$ . Since all the sensor coils have the same gains, the signal templates are collected from a single coil.

At each moment, the sensor array collects a set of magnetic signals, represented by  $\{s_i\}(i = 1, 2, \dots, 8)$ . For each signal  $s_i$ , we need to measure its similarities to the template signals  $\{t_m\}$ . To obtain a reliable and robust result, we test different signal transformation techniques in time series classification, including Fourier transform domain, power spectrum domain, auto-correlation domain. We eventually select two signal similarity measures. The first one is the cross-correlation between the signals ( $d_o(\cdot, \cdot)$ ), and the second one is the correlation between the signal derivatives ( $d_d(\cdot, \cdot)$ ). Their definitions are as follows:

$$\begin{aligned} d_o(s_i, t_m) &= \max(\text{corr}(s_i, t_m)) \\ d_d(s_i, t_m) &= \max(\text{corr}(\text{dir}(s_i), \text{dir}(t_m))) \end{aligned} \quad (6)$$

The operator  $\text{corr}(\cdot, \cdot)$  represents the cross-correlation between two signals, which quantifies their similarities. The

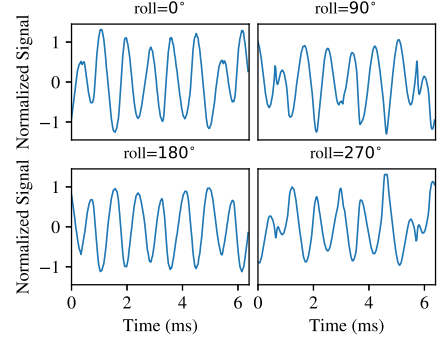


**Figure 6: Waveforms with Different Roll Angles.**

operator  $\text{dir}(\cdot, \cdot)$  represents taking derivative of the signal. In our implementation, we also use the bandpass filter centered around 1000Hz to remove signal noises. By computing the similarities between different signals and templates, we obtain the feature set.

The feature set contains rich information about the toothbrush roll angle. However, the relationship between the feature and the toothbrush roll angle is nonlinear, and many classifiers cannot handle the complexity. In our tests, the deep fully connected neural network achieves the best accuracy and robustness. This network contains four fully connected hidden layers with 32 neurons each. The output contains four classes of roll angles: left, right, up, and down. The classifier is trained by moving the toothbrush around with different roll angles to allow the sensors to collect the signals. This training process is conducted before system deployment so that no user participation is needed.

## 5 TOOTHBRUSHING MONITORING

To improve user convenience, we designed an unsupervised brushing surface recognition algorithm based on the spatial distribution of 15 tooth surfaces. To improve the algorithm robustness to user movements, we also developed an HMM-based algorithm to track the user’s motions.

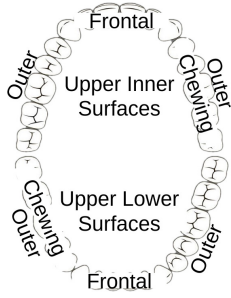
### 5.1 Preliminaries

**Tooth Surfaces.** As illustrated in Figure 7, a user’s left lower teeth include Left Lower Outer (LLO), Left Lower Chewing (LLC), and Left Lower Inner (LLI) surfaces. Similarly, the user’s left upper side, right lower side and right upper side also include outer, chewing, and inner surfaces. For the user’s front teeth, there are Front Lower Inner (FLI), Front Upper Inner (FUI), and Front Outer surfaces (FO). A complete list of tooth surfaces are listed in Table 1.

**Toothbrush Model.** Our motor tracking algorithm monitors the poses of the electric motor. We can use the motor pose to compute the pose of the brush head using the following equation.

$$[x', y', z'] = [x, y, z] + [l, 0, 0] * R_y(\beta) * R_z(\theta). \quad (7)$$

In this equation,  $l$  represents the distance between the brush head and the electric motor.  $R_y(\beta)$  and  $R_z(\theta)$  are rotation matrices, which are defined in Equation 2. We use  $[x', y', z', \beta, \theta]$  to represent the 5 DoF pose of the brush head.



Roll Angle	Surface List
up	LUC, RUC, FUI
down	LLC, RLC, FLI
right	LLO, LUO, RLI, RUI
left	LLI, LUI, RUO, RLO

**Figure 7: Toothbrush Roll Angles and Tooth Surfaces**

## 5.2 Unsupervised surface recognition

Let the toothbrush pose tracking results be denoted as  $\mathbf{X} = \{X_1, \dots, X_n\}$ , where  $X$  includes the  $x, y, z$  coordinates, and the roll angle of the toothbrush. Due to the spatial distribution of the teeth, the toothbrush poses form distinct clusters when brushing different surfaces, as illustrated in Figure 8. We model the distribution of the toothbrush poses within each cluster using a multivariate Gaussian distribution. We conducted a Shapiro-Wilk test, a classical approach to test the normality of data [14], on the data collected from five toothbrushing sessions. The mean p-value is 0.407, which is higher than the threshold value 0.05 that is needed to accept the normality assumption of data. In other words,  $P(X|M_t) \sim N(\mu_m, \Sigma_m)$ , where  $\mu$  represents the mean of the brush head positions, and  $\Sigma_m$  represents the covariance matrix. If the user is standing at location  $S_T$  and brushing surface  $m$ , then  $P(X|S_t, m)$  is the following Gaussian distribution:

$$P(X|S_t, m) = \frac{\exp(-\frac{1}{2}(X - \mu_m - S_t)^T \Sigma_m^{-1}(X - \mu_m - S_t))}{(2\pi)^{\frac{k}{2}} \det(\Sigma_m)^{\frac{1}{2}}} \quad (8)$$

Our goal is to recognize the brushing surfaces  $m$  based on the toothbrush poses  $X$ . There are two steps to achieving this goal. We firstly conduct a clustering of the toothbrush poses using the Expectation-Maximization algorithm (EM). Then we identify the tooth surface corresponding to each cluster by analyzing their spatial characteristics.

**Toothbrush Pose Clustering.** We use an EM-based algorithm for clustering. We repeat the expectation and maximization steps described in Equation 9 until convergence.

$$\begin{aligned} \text{Expectation : } P(m|X) &= \frac{N(X|\mu_m, \Sigma_m)}{\sum_k N(X|\mu_k, \Sigma_k)} \\ \text{Maximization : } \mu_m &= \frac{\sum_n P(m|X_n) X_n}{\sum_n P(m|X_n)} \\ \Sigma_m &= \frac{\sum_n P(m|X_n)(X_n - \mu_m)(X_n - \mu_m)^T}{\sum_n P(m|X_n)} \end{aligned} \quad (9)$$

Using this algorithm, we obtain the mean  $\mu_m$  and covariance matrix  $\Sigma_m$  for each cluster  $m$ . We also obtain the probability  $P(m|X)$ , which represents the likelihood for the head pose  $X$  to belong to a cluster  $m$ .

**Head Turn Detection.** When a user turns their head during brushing, the positions of the tooth surfaces change accordingly. To maintain recognition accuracy, we estimate the user’s tooth surface position after a head turn. The key

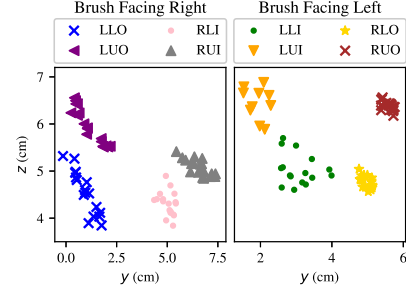


**Figure 8: Brush head positions for different surfaces.**

observation is that when the user brushes the back teeth, the motion direction of the toothbrush is approximately the same as the user’s facing direction.

In particular, we use the vector  $d$  to represent the facing direction of the user’s head, which is approximately equal to the primary axis of toothbrush motions. Therefore, for a cluster of toothbrush positions with a mean of  $\mu_m$  and covariance matrix  $\Sigma_m$ , we can estimate the facing direction  $d$  using the Principle Component Analysis (PCA), which is shown in the first line of Equation 10. Note that there are two feasible values for  $d$ , and we select the one that represents a smaller head turn angle.

$$\begin{aligned} d_m &\leftarrow \arg \max_d (d^T \Sigma_m d / d^T d) \\ \mu'_m &\leftarrow \mu_m - l * d_m / |d_m| + l * [-1, 0, 0]^T. \end{aligned} \quad (10)$$

Then we estimate the position of the tooth surface when the user is facing front, i.e., the head is facing the direction of  $[-1, 0, 0]$ , as illustrated in the coordinate system in Figure 2. This is achieved in the second line of Equation 10. In this equation,  $l$  is the distance between the tooth surface and the user’s neck. We empirically set its value to 10cm. We then use the cluster center  $\mu'_m$  to conduct tooth surface identification.

**Tooth Surface Identification.** The identification rules are as follows. First, depending on the toothbrush roll angle, we divide the clusters into four categories: the toothbrush bristles can face up, down, left, and right. The tooth surfaces for each toothbrush bristle directions are shown in Table 1. We next describe the surface identification rules for each toothbrush bristle orientation.

When the toothbrush bristle faces up, there are three possible surfaces: Left Upper Chewing (LUC), Right Upper Chewing (RUC), and Front Upper Inner (FUI) (shown in Table 1). To distinguish the front teeth, we observe that when the user brushes the front inner surfaces, the pitch angle is relatively large. Therefore, the algorithm selects the cluster center with the largest pitch angle, and assigns the surface label FUI. Then we compare the  $y$  coordinates of the remaining two clusters. Since the  $y$ -axis points to the right of the user, the cluster with the larger  $y$  coordinate is identified as RUC, and the other is identified as LUC. Using a similar rule, we can also identify the surface labels when the toothbrush bristle is facing down, i.e., the LLC, RLC, and FLI surfaces, as shown in Table 1. When the toothbrush bristle is facing right or left, we basically compute cluster centers to distinguish different surfaces, as illustrated in Figure 8.

### 5.3 User Location Tracking

To achieve robust surface recognition, it is important to distinguish a user’s head motion and the toothbrush motion. However, it is a challenging problem since only the toothbrush motion can be tracked. Fortunately, head motions of a user usually have unique patterns than toothbrush motions, which can be used to differentiate these two types of motions. For example, significant changes of the toothbrush location are often caused by location changes of the user, because the regular toothbrush movements when a user stands still are all in very short distances (the distance between the left and right teeth and the distance between the back and front teeth of an adult are less than 5cm for an adult [42, 65, 67]). Also, frequent movements in horizontal direction often indicate head movements or posture changes. We develop a Hidden Markov Model (HMM) based algorithm to detect these types of head movements.

**State Definition:** Each state,  $S_t$ , is defined as the 2D location of a user, as shown in the first row of Equation 11. We discretize the region in front of the sink so that there are in total  $N$  different states. Since we do not know the initial standing location of the user, we set the prior probability to be uniform, as shown in the second row of Equation 11. We set a uniform transition probability for the user to move to an adjacent or remain at the same location, as shown in the third row of Equation 11. We use the notation  $N(S_t)$  to represent all the states adjacent to  $S_t$  and the state  $S_t$  itself.

$$\begin{aligned} S_t &= [x_s, y_s] \\ \Pi(S_t) &= 1/N \\ P(S_t|S_{t-1}) &= \begin{cases} 1/|N(S_t)| & \text{if } S_t \in N(S_{t-1}) \\ 0 & \text{otherwise} \end{cases} \end{aligned} \quad (11)$$

**Emission Probability.** As discussed in the previous subsection, given the standing location of the user, the toothbrush poses form a mixture of Gaussian Distributions. The influence of the standing location is a translational shift. The emission probability can be computed as follows:

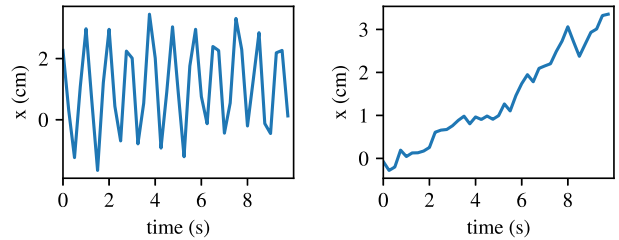
$$P(X|S_t) = \sum_{m=1}^{K_m} P(X|S_t, m). \quad (12)$$

The definition of  $P(X|S_t, m)$  is shown in Equation 8. Before tracking walking movements, we assume that the user brushes at least once without walking so that our system can estimate  $P(X|S = 0, m)$ ,  $\mu_m$ , and  $\Sigma_m$  at the user’s standing location. Then we can generate the emission probability by changing the value of  $S$  to the other standing locations.

Based on this HMM formulation, we use the classical Viterbi algorithm to find the most likely standing locations  $\{S_1, S_2, \dots, S_t\}$  based on the toothbrush pose measurements  $X$ . Then we use first row (Expectation step) in Equation 9 to calculate the probability for  $P(m|X)$ . The most likely surface  $m$  is returned as the surface recognition result.

### 5.4 Incorrect Toothbrushing Detection

**Aggressive Brushing Detection.** Aggressive toothbrushing involves periodic back and forth motions, which can be



(a) Aggressive Brushing (b) Normal Brushing  
Figure 9: Motions for Different Techniques

reflected by the toothbrush position changes, as shown in Figure 9a. On the other hand, when the user brushes using the correct technique that moves the brush head slowly, the  $x$  coordinate changes gradually. We detect aggressive brushing as follows. We compute the auto-correlation of the  $x$  coordinates within a time window of  $W$ . If the period is smaller than the threshold  $T_s$  and the moving distance is larger than a distance threshold  $T_d$ , then an aggressive brushing alert will be issued to the user.

**Under-brushing and over-brushing.** We compute the time spent on each surface based on the surface recognition algorithm described in this section. For each surface, if the time is larger than  $T_a$  or smaller than  $t_u$ , then the system will remind the user for over or under brushing, respectively. Since uneven brushing tends to have lower damage in the short term, our system will provide a toothbrushing report to the user after brushing is finished, so that the user can make up for the under-brushed surfaces, or be reminded to reduce brushing the over-brushed surfaces next time.

## 6 IMPLEMENTATION

We have considered different sensor options. The Hall-effect sensor, which is low-cost and widely available in mobile devices [28, 31, 36, 39, 73], does not meet the sensing requirements because it cannot detect fields weaker than  $0.1\mu T$ . Low-end magnetoresistive sensors, such as the KMI25/2, has a sensing dynamic range of less than  $188\mu T$  and high sensitivity to temperature changes. As a result, everyday magnetic materials, such as a metal shelf or jewelry, can cause the sensor to saturate. High-end magnetoresistive sensors, such as HMC1001, can meet the sensing requirements, yet they have high costs of above \$30 each. The fluxgate sensor has a similar sensing capability to the magnetic inductance sensor, and the main difference is that the fluxgate sensor can monitor the DC component of the magnetic field [50]. Since in monitoring electric toothbrushing, we are focused on the time-varying component of the magnetic field, we eventually select the low-cost (\$1<), flexible, highly-sensitive and reliable inductive sensor to develop our system.

According to Faraday’s law, the induced voltage in an inductance sensor is linearly proportional to the cross-section area of the coil and quadratic to the number of rounds. Furthermore, a ferromagnetic core can increase the induced voltage by 100 folds. As a trade-off between the size of the sensor and the sensing sensitivity, we custom-built coils with

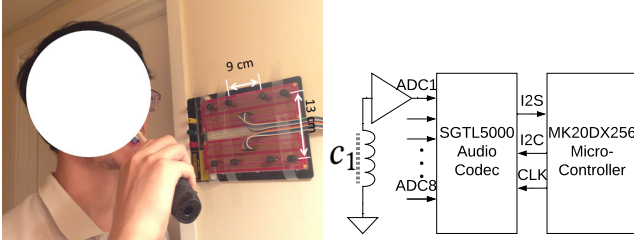


**Figure 10: Sensor Array** Figure 11: **Circuit Diagram** 3000 rounds and  $3\text{cm}^2$  cross-section areas, with a ferromagnetic core. A photo of the sensor array is shown in Figure 10.

The circuit diagram of the system is shown in Figure 11. To amplify the received magnetic signal, we use the low-noise MAX4466 amplifier, with amplification gain up to 60db. The multi-channel signals are digitized simultaneously using the 16 bits ADC on SGT5000 chips and transmitted to two MK20DX256 micro-controllers using the I2S protocol. A USB port from a computer powers our system. This can be replaced by a power cord from the charger of the toothbrush, which is typically placed near the sink in the bathroom. The SGT5000 costs \$1.27 each [13] and we used four. The MK20DX256 costs \$3.07 each [8] and we used two. The MAX4466 cost \$0.24 each [7] and we used eight.

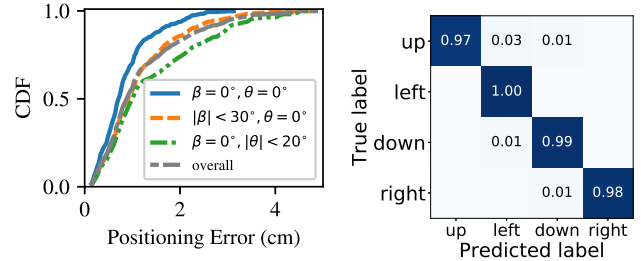
## 7 EVALUATION

### 7.1 6 DoF Pose Tracking

**Position Tracking Accuracy.** We firstly conducted a microbenchmark experiment to evaluate electric motor tracking accuracy. In this experiment, we placed the electric motor within the toothbrush at 32 positions, with x, y, and z coordinates ranging from 0 to 12 cm, 12 to 24 cm, and 0 to 4 cm, respectively. Meanwhile, we changed the motor orientation while it was in these positions. We adjusted the pitch angle  $\beta$  from -30 degree to 30 degrees, with 30 degrees apart, and the yaw angle  $\theta$  from -20 degree to 20 degrees, with 10 degrees apart. The tracking error is represented by the distance between the predicted position and the ground truth position.

The results are shown in Figure 12a. We can see that when the motor has no orientation changes, i.e.,  $\beta = 0$  and  $\theta = 0$ , the 90% percentile tracking error is 1.6 cm. When orientation changes, the tracking accuracy decreases slightly. When we changed the pitch angle  $\beta$  between  $-30^\circ$  and  $30^\circ$ , the 90% percentile error is 2.2cm. When the yaw angle  $\theta$  changed between  $[-20^\circ, 20^\circ]$ , the 90% percentile error is 3.0 cm. Although the tracking errors are sometimes larger than the distance between tooth surfaces, such as the 2-3 cm distance between the upper and lower surfaces, the system can still achieve correct detection because our algorithm is recognizing the tooth surfaces using the relative toothbrush positions, which are more robust than the absolute position tracking results.

**Roll Angle Estimation.** We next evaluated how accurately the system can recognize the motor roll angle. The data were collected when the users were brushing teeth, which involve rolling the toothbrush to clean different surfaces. In total,



(a) Tracking Error

(b) Roll Angle Estimation

### Figure 12: Toothbrush Pose Tracking

there are more than 100 minutes of data from 10 users, and over 18431 data points used in the evaluation. The results are shown in Figure 12b. We can see that the roll angle estimation algorithm is accurate: the recognition accuracy is above 97% for all the four roll angles. Since, during data collection, the toothbrush is moving around the users' teeth, it also demonstrates that the algorithm is robust to small position and orientation changes.

### 7.2 Toothbrushing Monitoring Functions

We recruited 14 volunteers and let each volunteer brush 5-10 sessions, each session ranging from 1 minute to 4 minutes. An observer recorded all the toothbrushing surface ground truths. The volunteers included three females and eleven males, with heights ranging from 155 cm to 185 cm. We adjusted the aligned the system according to each user's height. Ten participants were in late twenties, one was in late thirties, and three were in late fifties. To enable the evaluation of uneven brushing detection, we set different brushing duration requirements for different surfaces. We labeled brushing for over 10 seconds as over-brushing, and below 5 seconds as under-brushing. In total, we have recorded 102 toothbrushing sessions. Each user tried to stay in the same location each time, but there were no deliberate measurements for the user standing locations. As a result, small variations did exist.

**Surface Recognition** The overall toothbrushing surface recognition results are shown in Figure 13. The surface recognition precision, recall, and f1 scores are 85.4%, 85.5%, and 85.4%, respectively. We can see that in general, most brushing surfaces are correctly recognized.

We can see that a major source of error is that difficulties in differentiating upper or lower surfaces. For example, there are 21.5% of wrong recognition from Right Lower Inner (RLI) to Right Upper Inner (RUI), and 19.4% of the opposite direction. There are also 8.8% of wrong recognition from Left Lower Outer (LLO) to Left Upper Outer (LUO), and 6.6% of the opposite direction. This is because, in some cases, the distances between the upper and lower surfaces are small so that they can introduce errors. In the future, we will consider sensing the fine-grained roll angle of the toothbrush to assist in addressing these cases.

We can also see cases when the algorithm confuses left and right surfaces. For example, there are 14.2% of incorrect

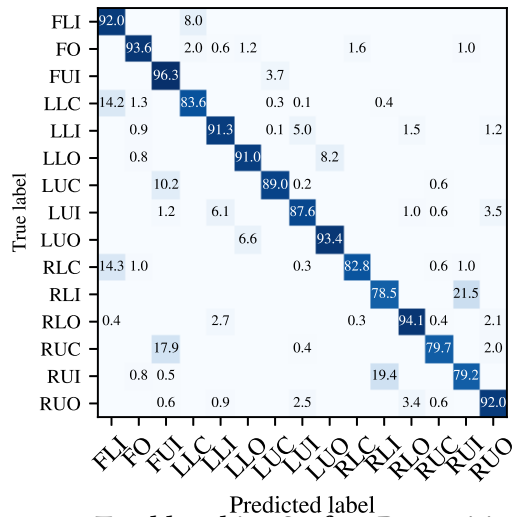


Figure 13: Toothbrushing Surface Recognition (%)

recognition that confuses Left Lower Chewing (LLC) with the Front Lower Inner (FLI), and 14.3% of incorrect recognition that confuses Right Lower Chewing (RLC) with the Front Lower Inner (FLI). Similarly, there are recognition errors between FUI, RUC, and LUC. The system rely on the horizontal coordinates of the toothbrush poses to differentiate these surfaces, and wrong recognition results occur when the tracking error is larger than the horizontal distance between the tooth surfaces, which is about 5cm between the left and the right teeth.

We also investigated how individual variations influence the surface recognition accuracy. In Figure 14, we plot the surface detection precision, recall, and f1 scores for all the 14 users with and without head pose and location tracking. We can see that there are two users (13 and 14), achieving over 90% of the surface recognition f1 score. The detection accuracies for different users vary between around 70% to 95%. The monitoring accuracy variations among different users are caused by many factors, including mouth structure, the distance between a user and the sensor, user movements during brushing, and personal brushing habits. Actually personal brushing gestures can influence recognition accuracy. We noticed that some users slightly raised their heads when brushing the lower surfaces, and then lowered their heads when brushing the upper surfaces. As a result, the toothbrush pose estimations of the upper and lower surfaces are sometimes inaccurate. Also, some user tilted his head during brushing, which caused some incorrect surface recognition results. This suggests that a personalized surface recognition algorithm could be useful for many users.

We can also see that the tracking-based approach can improve the recognition of F1 scores for most of the users. When the user moves during brushing, the tracking based algorithm begins to achieve better performance. We can see that for user 2 and user 7, the HMM algorithm achieves 5% and 6% than the basic algorithm, because these two users moved their standing locations during brushing.

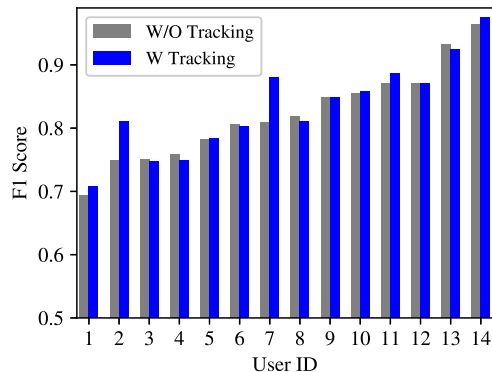


Figure 14: Surface Recognition Accuracy vs. Users Incorrect Toothbrushing Detection.

Our goal is to detect aggressive brushing, over brushing, and under brushing. To evaluate aggressive brushing detection, we conducted an additional experiment that includes ten toothbrushing sessions, with the user brushing teeth using back-forth motions. In total, there are 120 instances of aggressive brushing, and 740 instances of normal brushing. Then we evaluated whether our algorithm can differentiate aggressive brushing data from other normal brushing data. To evaluate over/under brushing, we use the same dataset described in the previous section. Specifically, there are 452, 190, and 101 instances of normal, over, and under brushing in the dataset, respectively.

The incorrect toothbrushing detection results are shown in Figure 15. We can see that the f1 scores of detection for over-brushing, under-brushing, and aggressive brushing are 93.2%, 87.4%, and 92%, respectively. Since the over-brushing and aggressive brushing are potentially more damaging, we need to alert the user immediately once they are detected. The miss detection rates, which equal 1 minus recall rates, for over-brushing and aggressive brushing are 10% and 8%, respectively. On the other hand, the under-brushing cause less immediate damage, so the system can aggregate the toothbrushing data over several brushing sessions, and remind the user to increase brushing time for specific surfaces.

**Comparison with Commercial Systems.** Next, we tested two existing commercial systems. Our goal is to provide a baseline comparison between our magnetic sensing based system with existing camera and IMU-based systems. Oral B and Kolibree electric toothbrushes were used in this test. Oral B system used a smartphone camera to monitor the user’s toothbrushing, while Kolibree used the toothbrush onboard IMU sensors. Both systems only detected brushing quadrants or sextants instead of tooth surfaces, as each quadrant of the teeth contains three surfaces. For example, the left upper quadrant contains LUO, LUC, and LUI surfaces. To compare with these systems, we adjusted our algorithm to generate quadrant recognition results.

In this experiment, we used an Oral B toothbrush to brush three times, and used our system and the Oral B app to monitor the toothbrushing concurrently. Then we used the Kolibree app to monitor toothbrushing with the Kolibree toothbrush separately. The detection results are shown in

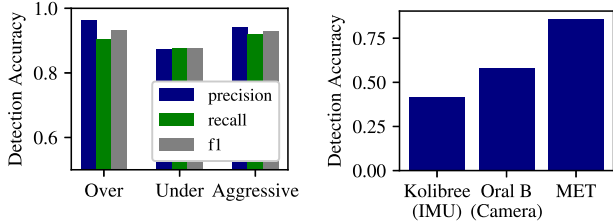
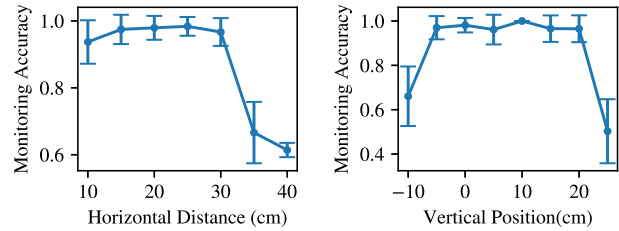


**Figure 15: Incorrect Brush-Figure 16: MET vs. Commercial Detection**

Figure 16. We can see that our system outperforms these two systems. We can see that Kolibree and Oral B achieve 41% and 58% of accuracy, respectively. On the other hand, MET achieves 86% of detection accuracy. During the experiment, we observe some drawbacks of the existing systems. The Kolibree toothbrush accurately tracked the toothbrush roll angle, but it was insensitive to the subtle brushing position changes under mechanical vibrations during electric toothbrushing. As a result, it has large errors in differentiating the left, right, up, and down surfaces that have the same roll angle. The Oral B system requires careful alignment of the user’s head position each time before brushing: the user needs to make sure their face appears inside a small area within the camera image. In general, it can differentiate different tooth quadrants. However, the system does not perform well when there are variations in the toothbrush orientation: a small change in the toothbrush yaw angle can confuse the system between left and right quadrants. Similarly, a small change in the toothbrush pitch angle can confuse the system about the upper and lower quadrants. Its performances degrade would further when the user moves or in poor lighting conditions.

**Monitoring Range** We conducted experiments to test the range for the system to achieve reliable monitoring. In the first experiment, we gradually increased the horizontal distance between the user’s chin and the sensor, and conducted toothbrushing for four times at each distance. The mean and variance of the surface recognition accuracy are shown in Figure 17a. We can see that when the distance is less than 30 cm, the system maintains over 90% of monitoring accuracy. When the distance is larger 35 cm, the monitoring accuracy begins to drop, and the variations also increase. Since the typical sizes of bathroom sinks include 24, 30, and 33 inches, when the user is brushing at the middle of the sink, our system can still maintain a good monitoring performance.

In the second experiment, we tested the monitoring accuracy when we adjust the vertical alignment between the sensor and the user, and the results are shown in Figure 17b. We define the vertical position as the difference between the user’s chin’s height and the height of the lower row of the sensors. We can see that when the vertical position is between -5 cm to 20 cm, the monitoring accuracy is above 90%. When the position is below -5 cm or above 25 cm, the monitoring accuracy drops to about 70% and 50%. The vertical monitoring range is sufficient to handle the issue of a



**(a) Accu. vs. Horizontal Dist. (b) Accu. vs. Vertical Dist. Figure 17: Toothbrushing Monitoring Performance**

user changing height when brushing teeth, such as wearing different shoes. Plus, the system will benefit from a user-friendly wall mount that can be adjusted according to the height of the user.

### 7.3 Environmental and Battery Factors

**Environmental Magnetic Noise.** We next tested the background magnetic noises at four rooms, two bathrooms, and two offices, where we conducted experiments. We recorded the background magnetic noises and plotted the power spectrums in Figure 18. We can see that at bathroom 1 (B1) and office 1 (O1), there is a large peak at 64 Hz, which corresponds to the powerline magnetic field. B2 and O2 have much lower magnetic noises of less than  $10^{-5}$  W/Hz. For all these rooms, the magnetic noises at about 1000 Hz are lower than  $10^{-3}$  W/Hz, which are two magnitudes of orders weaker than the electric motor magnetic field, as illustrated earlier in Figure 3c. We also observe that the background noise has temporal stability, as reported in earlier works [51, 53, 70].

We also tested if normal metal objects will influence the monitoring results. These rooms had different layouts and were normally furnished with metallic objects, including tables with iron legs, mirrors, faucets. We also tested placing different objects near the user, including a metal plate, jewelry, and a metal cup. The magnetic fields experience no absorption by the human body, so the user’s hand, tongue, or head does not influence the motor position tracking [19]. One of the users had a tooth implant, which contained zirconium and titanium. We have not observed any negative effects on the monitoring system.

**Influence of Battery Level.** We experimented to test the influence of the battery level on the motor magnetic field. We placed the toothbrush at a fixed location and turn it on continuously for 30+ minutes, and recorded the signal RMS 5 times each second. The results are shown in Figure 19. We can see that the RMS of the motor magnetic field remains stable for about 1500 seconds. There are small fluctuations from time to time. The motor rotation speed occasionally drops for a very short period (<0.3s), possibly due to motor overheating. This causes some fluctuations in the RMS values. In MET, we discard magnetic signals that have excessively low frequencies (below 1000 Hz). After about 25 minutes, the RMS value drops noticeably due to the low battery levels. Since each toothbrushing session lasts for about 2 minutes, the battery life of the toothbrush is long enough

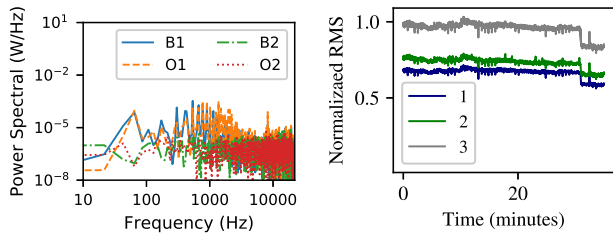


**Figure 18: Noise Spectrum** **Figure 19: Battery vs. Time** to allow accurate tracking of our system. Besides, we have not observed any significant mechanical deterioration that influences tracking in the past 2 years .

#### 7.4 Extension to Other Toothbrush Models

We observed that many other models of electric toothbrushes generate time-varying magnetic fields that can be used for position tracking. In a preliminary experiment, we tested if we can generalize our system to achieve 1-d position tracking for different electric motors. In particular, aside from the Oral-B genius 7000 (OB1) [9] we used in this paper, we also tested Oral-B White Pro 1000 (OB2) [10], Spinbrush Pro clean (SP) [15], Phillips Sonicare (Phillips) [12], and Curaprox Hydrosonic (Cura) [2]. For each model of the electric toothbrush, we constructed a basic linear regression model that maps the magnetic field strength to the distance between the sensor and toothbrush. We then slowly moved the toothbrush from 10 cm to 60 cm, and used the model to predict the distance. The results were shown in Figure 20. We can see that the tracking errors are less than 5cm for most of the time. The tracking errors are smaller when the distance is less than 50cm. When the distance is larger than 55cm, we can see that the tracking errors increase to about 5cm. This is because, at this distance, the background magnetic noises become significant compared with the motor magnetic field.

### 8 RELATED WORK

**Toothbrushing Monitoring.** Inertia sensors have been used in toothbrush and [49] wearable wristband [39, 40] to monitor toothbrushing motions. Acoustic sensors are also used to monitor toothbrushing [44, 59, 63]. However, these systems do not achieve good performance for electric toothbrushing monitoring. A main reason is that the electric motor generates vibration motions and acoustic noises, which cause significant errors for motion sensing and acoustic sensing based approaches. Camera based systems have been designed [27, 79], but these systems suffer from the visibility obstruction when the user puts the toothbrush inside the mouth. As a result, they only achieve coarse-grained brushing region recognition. Different from all the existing toothbrushing monitoring system, MET does not have these limitations, and it performs passive monitoring on unmodified electric toothbrushes with high accuracy and low cost.

**Magnetic Sensing.** Magnetic sensing has been used for near-field communication [64], vehicle status monitoring [62], and daily activity recognition [45]. Due to its accuracy and robustness, magnetic sensing has also been successfully

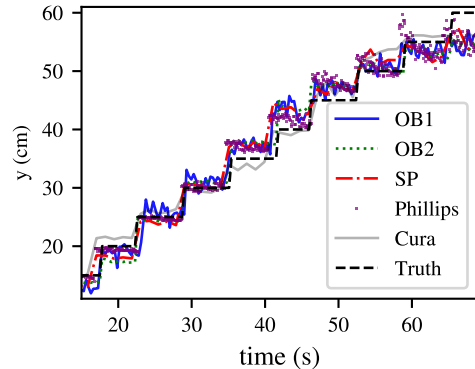


**Figure 20: Tracking Different Electric Toothbrushes** applied in position tracking [24, 32, 58, 77]. Many works are leveraging static or low-frequency magnetic fields to achieve positioning. There are cooperative localization approaches that attach specialized magnetic sources, such as regular-shaped magnets or magnetic coils connected with sinusoidal currents, to the subjects to generate tracking signals [19, 20, 28, 56]. While these approaches can achieve high tracking precision and orientation tracking, the requirement for the subject to cooperate by attaching additional transmitting devices limits its scalability, especially for our application. In order to eliminate the requirement for additional hardware for tracking signals, the non-cooperative approach achieves localization through the sensing of the existing magnetic fields of the subjects [53, 74]. Prior works construct statistical signatures to model the existing magnetic field to achieve localization, yet these algorithms have lower tracking granularities, and are focused on the 2D position tracking. In our application, the toothbrush has 6 DoF motions, and the tracking granularity needs to be centimeter level. In comparison, our system is the first to perform tracking based on sensing the existing magnetic fields from an unmodified electric motor, which is a non-cooperating magnetic source, and achieves a centimeter-level of tracking granularity and orientation tracking.

### 9 CONCLUSION AND FUTURE WORK

We present MET - an electrical toothbrushing monitoring system that essentially tracks the 6 DoF of the toothbrush by sensing the magnetic field generated by the DC motor of the toothbrush. Compared with existing systems that rely on the camera, acoustic, and inertial sensing, magneto-inductive sensing can achieve higher precision, thus introducing rich monitoring functions at a very low cost. MET is evaluated in realist settings and users, and evaluation results show that MET recognizes the toothbrushing surfaces with an accuracy of 85.2%, significantly outperforming existing monitoring systems. Furthermore, the techniques developed in this work for recognition with correlated context can be applied in a broader setting. In the future work, we will consider combining our magnetic sensing techniques with other sensing modalities, such as cameras, IMU sensors, and acoustic sensors, to further improve the position tracking granularity to tooth level. We will also explore more user-friendly designs.

## REFERENCES

- [1] Cavities/tooth decay. <https://www.mayoclinic.org/diseases-conditions/cavities/symptoms-causes/syc-20352892>.
- [2] Curaprox hydrosonic toothbrush. <https://www.curaprox.com/us-en/hydrosonic-toothbrush>. Accessed: 2019-12-10.
- [3] Guidelines for using an electric toothbrush. <https://oralb.com/en-us/oral-health/solutions/electric-toothbrushes/using-rechargeable-electric-toothbrush>.
- [4] How to brush teeth properly? <https://www.oralb.co.uk/en-gb/oral-health/solutions/electric-toothbrushes/how-to-brush-teeth-properly>.
- [5] How to use your electric toothbrush properly. <https://www.goodhousekeeping.com/uk/health/health-advice/a562902/how-to-use-your-electric-toothbrush-properly/>.
- [6] Kolibree electric toothbrushes. <https://www.kolibree.com/en/>.
- [7] Max4466. [https://www.maximintegrated.com/en/products/analog/audio/MAX4466.html/tb\\_tab3](https://www.maximintegrated.com/en/products/analog/audio/MAX4466.html/tb_tab3).
- [8] Mk20dx256 datasheet. <https://www.nxp.com/docs/en/data-sheet/K20P64M72SF1.pdf>.
- [9] Oral-b genius 7000 rechargeable electric toothbrush. <https://oralb.com/en-us/products/electric-toothbrushes/7000-wireless-smartguide-plus-electric-toothbrush>.
- [10] Oral-b pro 1000 electric toothbrush. <https://oralb.com/en-us/products/electric-toothbrushes/professional-care-1000-toothbrush>. Accessed: 2019-12-10.
- [11] Philips electric toothbrushes. <https://www.usa.philips.com/c-m-pe/electric-toothbrushes>.
- [12] Philips sonicare flexcare platinum. [https://www.usa.philips.com/c-p/HX9110\\_02/sonicare-flexcare-platinum-sonic-electric-toothbrush/support](https://www.usa.philips.com/c-p/HX9110_02/sonicare-flexcare-platinum-sonic-electric-toothbrush/support). Accessed: 2019-12-10.
- [13] Sglt5000. [https://www.nxp.com/products/audio/audio-converters/ultra-low-power-audio-codec:SGTL5000?tab=Buy\\_Parametric\\_Tab&fromSearch=false#](https://www.nxp.com/products/audio/audio-converters/ultra-low-power-audio-codec:SGTL5000?tab=Buy_Parametric_Tab&fromSearch=false#/).
- [14] Shapiro's Wilk test for data distribution normality. [https://en.wikipedia.org/wiki/Shapiro%E2%80%93Wilk\\_test](https://en.wikipedia.org/wiki/Shapiro%E2%80%93Wilk_test).
- [15] Spinbrush pro clean. <https://www.armandhammer.com/spinbrush-pro-clean>. Accessed: 2019-12-10.
- [16] Bleeding gums, eroded enamel and even fillings falling out - how your electric toothbrush can destroy your teeth. 2016.
- [17] Millennials in the u.s.: Consumer goods and shopping behavior. 2017.
- [18] P. A., S. M., and H. D. et al. Stimulation of salivary flow with a powered toothbrush in a xerostomic population. In *Special care in dentistry*, 2006.
- [19] T. E. Abrudan, Z. Xiao, A. Markham, and N. Trigoni. Distortion rejecting magneto-inductive three-dimensional localization (magloc). *IEEE Journal on Selected Areas in Communications*, 33(11):2404–2417, 2015.
- [20] T. E. Abrudan, Z. Xiao, A. Markham, and N. Trigoni. Underground incrementally deployed magneto-inductive 3-d positioning network. *IEEE Transactions on Geoscience and Remote Sensing*, 54(8):4376–4391, 2016.
- [21] A. Ackva, G. Ombach, and J. Junak. Numerical coupled analysis of dc motors including saturation and commutation effects. In *2005 European Conference on Power Electronics and Applications*, pages 6–pp. IEEE, 2005.
- [22] R. H. Affoo, K. Trottier, R. Garrick, T. Mascarenhas, Y. Jang, and R. E. Martin. The effects of tooth brushing on whole salivary flow rate in older adults. In *BioMed research international*, 2018.
- [23] J. Asadoorian. Cdha position paper on tooth brushing. *CJDH*, 40, 11 2005.
- [24] N. T. B. Wei and A. Markham. imag: Accurate and rapidly deployable inertial magneto-inductive localisation. *IEEE Intl Conference on Robotics and Automation (ICRA)*, 2018.
- [25] M. e. a. Bizhang. Toothbrush abrasivity in a long-term simulation on human dentin depends on brushing mode and bristle arrangement. In *PLoS one*. IEEE, 2017.
- [26] N. Boules. Design optimization of permanent magnet dc motors. *IEEE Transactions on Industry Applications*, 26(4):786–792, 1990.
- [27] Y.-C. Chang, J.-L. Lo, C.-J. Huang, N.-Y. Hsu, H.-H. Chu, H.-Y. Wang, P.-Y. Chi, and Y.-L. Hsieh. Playful toothbrush: ubicomp technology for teaching tooth brushing to kindergarten children. In *Proceedings of the SIGCHI conference on human factors in computing systems*, pages 363–372. ACM, 2008.
- [28] K.-Y. Chen, K. Lyons, S. White, and S. Patel. utrack: 3d input using two magnetic sensors. In *Proceedings of the 26th annual ACM symposium on User interface software and technology*, pages 237–244. ACM, 2013.
- [29] J. Cros, G. Sincero, and P. Viarouge. Design method for brush permanent magnet dc motors. In *2009 IEEE International Electric Machines and Drives Conference*, pages 1625–1632. IEEE, 2009.
- [30] J. Cros, P. Viarouge, and A. Halila. Brush dc motors with concentrated windings and soft magnetic composites armatures. In *Conference Record of the 2001 IEEE Industry Applications Conference. 36th IAS Annual Meeting (Cat. No. 01CH37248)*, volume 4, pages 2549–2556. IEEE, 2001.
- [31] A. Farajidavar, J. M. Block, and M. Ghovanloo. A comprehensive method for magnetic sensor calibration: A precise system for 3-d tracking of the tongue movements. In *Engineering in Medicine and Biology Society (EMBC), 2012 Annual International Conference of the IEEE*, pages 1153–1156. IEEE, 2012.
- [32] A. Franz, T. Haidegger, W. Birkfellner, K. Cleary, T. M Peters, and L. Maier-Hein. Electromagnetic tracking in medicine-a review of technology, validation, and applications. 2014.
- [33] J. F. Gieras, C. Wang, and J. C. Lai. *Noise of polyphase electric motors*. CRC press, 2018.
- [34] L. Gu, D. Jia, P. Vicaire, T. Yan, L. Luo, A. Tirumala, Q. Cao, T. He, J. A. Stankovic, T. Abdelzaher, and B. H. Krogh. Lightweight detection and classification for wireless sensor networks in realistic environments. In *Proceedings of the 3rd International Conference on Embedded Networked Sensor Systems, SenSys '05*, 2005.
- [35] H. G. H., B. H. S., V. E. C. I., and A. A. V. N. Toothbrushing affects the protein composition of whole saliva. In *European Journal of Oral Sciences*, 2002.
- [36] X. Han, H. Seki, Y. Kamiya, and M. Hikizu. Wearable handwriting input device using magnetic field: 2nd report: Influence of misalignment of magnet and writing plane. *Precision Engineering*, 34(3):425–430, 2010.
- [37] R. J. Hawkins, D. L. Zanetti, P. A. Main, D. F. Otchere, J. J. Dwyer, A. Jokovic, and D. Locker. Toothbrushing competency among high-risk grade one students: an evaluation of two methods of dental health education. *Journal of public health dentistry*, 61(4):197–202, 2001.
- [38] T. He, S. Krishnamurthy, L. Luo, T. Yan, L. Gu, R. Stoleru, G. Zhou, Q. Cao, P. Vicaire, J. A. Stankovic, T. F. Abdelzaher, J. Hui, and B. Krogh. Vigilnet: An integrated sensor network system for energy-efficient surveillance. *ACM Trans. Sen. Netw.*
- [39] H. Huang and S. Lin. Toothbrushing monitoring using wrist watch. In *Proceedings of the 14th ACM Conference on Embedded Network Sensor Systems CD-ROM, SenSys '16*, pages 202–215, New York, NY, USA, 2016. ACM.
- [40] H. Huang and S. Lin. Toothbrushing recognition using neural networks. In *2017 IEEE/ACM Second International Conference on Internet-of-Things Design and Implementation (IoTDI)*, pages 309–310. IEEE, 2017.
- [41] Y. Jain. A comparison of the efficacy of powered and manual toothbrushes in controlling plaque and gingivitis: a clinical study. In *Clinical, cosmetic and investigational dentistry*, 2013.
- [42] N. Khare, S. B. Patil, S. M. Kale, J. Sumeet, I. Sonali, and B. Sumeet. Normal mouth opening in an adult indian population. *Journal of maxillofacial and oral surgery*, 11(3):309–313, 2012.
- [43] J. Korpela, R. Miyaji, T. Maekawa, K. Nozaki, and H. Tamagawa. Evaluating tooth brushing performance with smartphone sound data. In *Proceedings of the 2015 ACM International Joint Conference on Pervasive and Ubiquitous Computing, UbiComp '15*, 2015.

- [44] J. Korpela, R. Miyaji, T. Maekawa, K. Nozaki, and H. Tamagawa. Toothbrushing performance evaluation using smartphone audio based on hybrid hmm-recognition/svm-regression model. *Journal of Information Processing*, 24(2):302–313, 2016.
- [45] G. Laput, C. Yang, R. Xiao, A. Sample, and C. Harrison. Em-sense: Touch recognition of uninstrumented, electrical and electromechanical objects. In *Proceedings of the 28th Annual ACM Symposium on User Interface Software & Technology*, pages 157–166. ACM, 2015.
- [46] C.-I. Lee and G.-H. Jang. Experimental measurement and simulated verification of the unbalanced magnetic force in brushless dc motors. *IEEE Transactions on Magnetics*, 44(11):4377–4380, 2008.
- [47] J.-W. Lee, K.-H. Lee, K.-S. Kim, D.-J. Kim, and K. Kim. Development of smart toothbrush monitoring system for ubiquitous healthcare. In *2006 International Conference of the IEEE Engineering in Medicine and Biology Society*, pages 6422–6425. IEEE, 2006.
- [48] Y. J. Lee, P. J. Lee, K. S. Kim, W. Park, K. D. Kim, D. Hwang, and J. W. Lee. Toothbrushing region detection using three-axis accelerometer and magnetic sensor. *IEEE Transactions on Biomedical Engineering*, 2012.
- [49] Y.-J. Lee, P.-J. Lee, K.-S. Kim, W. Park, K.-D. Kim, D. Hwang, and J.-W. Lee. Toothbrushing region detection using three-axis accelerometer and magnetic sensor. *IEEE Transactions on Biomedical Engineering*, 59(3):872–881, 2012.
- [50] J. Lenz and S. Edelstein. Magnetic sensors and their applications. *IEEE Sensors journal*, 6(3):631–649, 2006.
- [51] B. Li, T. Gallagher, A. G. Dempster, and C. Rizos. How feasible is the use of magnetic field alone for indoor positioning? In *2012 International Conference on Indoor Positioning and Indoor Navigation (IPIN)*, pages 1–9. IEEE, 2012.
- [52] C. B. Lourenço, M. V. Saintrain, and A. P. Vieira. Child, neglect and oral health. In *BMC pediatrics*, 2013.
- [53] C. X. Lu, Y. Li, P. Zhao, C. Chen, L. Xie, H. Wen, R. Tan, and N. Trigoni. Simultaneous localization and mapping with power network electromagnetic field. In *Proceedings of the 24th Annual International Conference on Mobile Computing and Networking*, pages 607–622. ACM, 2018.
- [54] I. Macgregor and A. Rugg-Gunn. Survey of toothbrushing duration in 85 uninstructed english schoolchildren. *Community dentistry and oral epidemiology*, 7(5):297–298, 1979.
- [55] A. Markham, N. Trigoni, S. A. Ellwood, and D. W. Macdonald. Revealing the hidden lives of underground animals using magneto-inductive tracking. In *Proceedings of the 8th ACM Conference on Embedded Networked Sensor Systems, SenSys '10*, 2010.
- [56] A. Markham, N. Trigoni, S. A. Ellwood, and D. W. Macdonald. Revealing the hidden lives of underground animals using magneto-inductive tracking. In *Proceedings of the 8th ACM Conference on Embedded Networked Sensor Systems*, pages 281–294. ACM, 2010.
- [57] A. Markham, N. Trigoni, D. Macdonald, and S. A. Ellwood. Underground localization in 3-d using magneto-inductive tracking. *Sensors Journal, IEEE*, 2012.
- [58] N. Marquardt, A. S. Taylor, N. Villar, and S. Greenberg. Rethinking rfid: Awareness and control for interaction with rfid systems. In *Proceedings of the SIGCHI Conference on Human Factors in Computing Systems, CHI '10*, 2010.
- [59] C.-H. Min, N. F. Ince, and A. H. Tewfik. Early morning activity detection using acoustics and wearable wireless sensors. In *2008 16th European Signal Processing Conference*, pages 1–5. IEEE, 2008.
- [60] T. Nara, S. Suzuki, and S. Ando. A closed-form formula for magnetic dipole localization by measurement of its magnetic field and spatial gradients. *IEEE Transactions on Magnetics*, 42(10):3291–3293, 2006.
- [61] P. Nguyen, H. Nguyen, D. Nguyen, T. N. Dinh, H. M. La, and T. Vu. Parksense: Automatic parking positioning by leveraging in-vehicle magnetic field variation. *IEEE Access*, 2017.
- [62] P. Nguyen, H. Nguyen, D. Nguyen, T. N. Dinh, H. M. La, and T. Vu. Parksense: automatic parking positioning by leveraging in-vehicle magnetic field variation. *IEEE Access*, 5:25021–25033, 2017.
- [63] Z. Ouyang, J. Hu, J. Niu, and Z. Qi. An asymmetrical acoustic field detection system for daily tooth brushing monitoring. In *GLOBECOM 2017-2017 IEEE Global Communications Conference*, pages 1–6. IEEE, 2017.
- [64] H. Pan, Y.-C. Chen, G. Xue, and X. Ji. Magnecomm: Magnetometer-based near-field communication. In *Proceedings of the 23rd Annual International Conference on Mobile Computing and Networking*, pages 167–179. ACM, 2017.
- [65] J. P. Pillai, R. A. Patel, A. M. Banker, J. Rajarajeswari, et al. Correlation between maxillary central incisor crown form and maxillary dental arch form: A model-based morphometric, cross-sectional study. *Journal of Forensic Science and Medicine*, 4(2):70, 2018.
- [66] G. Pirkel, P. Hevesi, J. Cheng, and P. Lukowicz. mbeacon: Accurate, robust proximity detection with smart phones and smart watches using low frequency modulated magnetic fields. In *Proceedings of the 10th EAI International Conference on Body Area Networks, BodyNets '15*, 2015.
- [67] G. Placko, V. Bellot-Samson, S. Brunet, L. Guyot, O. Richard, F. Cheynet, C. Chossegros, and M. Ouaknine. Normal mouth opening in the adult french population. *Revue de stomatologie et de chirurgie maxillo-faciale*, 106(5):267–271, 2005.
- [68] V. Priya Murali, J. Joseph, and K. Ken Ostrikov. *Electromagnetic Field Sensors: Fundamentals, Properties, and Applications*. 2018.
- [69] A. Rugg-Gunn and I. MacGregor. A survey of toothbrushing behaviour in children and young adults. *Journal of Periodontal Research*, 13(4):382–389, 1978.
- [70] W. Shao, F. Zhao, C. Wang, H. Luo, T. Muhammad Zahid, Q. Wang, and D. Li. Location fingerprint extraction for magnetic field magnitude based indoor positioning. *Journal of Sensors*, 2016, 2016.
- [71] G. Sincero, J. Ghannou, J. Cros, and P. Viarouge. Collector model for simulation of brush machines. *Mathematics and Computers in Simulation*, 81(2):340–353, 2010.
- [72] G. C. Sincero, J. Cros, and P. Viarouge. Efficient simulation method for comparison of brush and brushless dc motors for light traction application. In *2009 13th European Conference on Power Electronics and Applications*, pages 1–10. IEEE, 2009.
- [73] E. Stathopoulos, V. Schlageter, B. Meyrat, Y. Ribaupierre, and P. Kucera. Magnetic pill tracking: a novel non-invasive tool for investigation of human digestive motility. *Neurogastroenterology & Motility*, 17(1):148–154, 2005.
- [74] S. Taghvaeeyan. Exploiting inherent magnetic signatures of ferromagnetic objects for detection, identification, and position estimation applications. 2014.
- [75] A. Vibhute and K. L. Vandana. The effectiveness of manual versus powered toothbrushes for plaque removal and gingival health: A meta-analysis. *Journal of Indian Society of Periodontology*, 2012.
- [76] P. Vijayraghavan and R. Krishnan. Noise in electric machines: A review. *IEEE Transactions on Industry Applications*, 35(5):1007–1013, 1999.
- [77] N. Wahlström and F. Gustafsson. Tracking position and orientation of magnetic objects using magnetometer networks. 2015.
- [78] B. Wei, N. Trigoni, and A. Markham. imag: Accurate and rapidly deployable inertial magneto-inductive localisation. In *2018 IEEE International Conference on Robotics and Automation (ICRA)*, 2018.
- [79] T. Yoshitani, M. Ogata, and K. Yatani. Lumio: A plaque-aware toothbrush. In *Proceedings of the 2016 ACM International Joint Conference on Pervasive and Ubiquitous Computing, UbiComp '16*, pages 605–615, New York, NY, USA, 2016. ACM.
- [80] A. Zaki and S. Ibrahim. Modeling and analysis of pm brushed dc motor using fem. In *2005 European Conference on Power Electronics and Applications*, pages 6–pp. IEEE, 2005.